

Article

Study of the Overflow Transport of the Nordic Sea

Wenqi Shi ^{1,*}, Ning Li ^{2,*} and Xianqing Lv ^{3,4}¹ National Marine Environmental Monitoring Center, Dalian 116023, China² School of Science, Dalian Jiaotong University, Dalian 116028, China³ Physical Oceanography Laboratory, CIMST, Ocean University of China, Qingdao 266100, China; xqinglv@ouc.edu.cn⁴ Qingdao National Laboratory for Marine Science and Technology, Qingdao 266100, China

* Correspondence: swqouc@163.com (W.S.); lndjtu@163.com (N.L.); Tel.: +86-1347-842-3671 (W.S.); +86-1584-261-1706 (N.L.)

Abstract: Changes in the climate system over recent decades have had profound impacts on the mean state and variability of ocean circulation, while the Nordic Sea overflow has remained stable in volume transport during the last two decades. The changes of the overflow flux depend on the pressure difference at the depth of the overflow outlet on both sides of the Greenland-Scotland Ridge (GSR). Combining satellite altimeter data and the reanalysis hydrological data, the analysis found that the barotropic pressure difference and baroclinic pressure difference on both sides of the GSR had a good negative correlation from 1993 to 2015. Both are caused by changes in the properties of the upper water, and the total pressure difference has no trend change. The weakening of deep convection can only change the temperature and salt structure of the Nordic Sea, but cannot reduce the mass of the water column. Therefore, the stable pressure difference drives a stable overflow. The overflow water storage in the Nordic Sea is decreasing, which may be caused by the reduction of local overflow water production and the constant overflow flux. When the upper interface of the overflow water body in the Nordic Sea is close to or below the outlet depth, the overflow is likely to greatly slow down or even experience a hiatus in the future, which deserves more attention.

Keywords: Nordic Sea; overflow flux; barotropic pressure; baroclinic pressure



Citation: Shi, W.; Li, N.; Lv, X. Study of the Overflow Transport of the Nordic Sea. *Water* **2021**, *13*, 2675. <https://doi.org/10.3390/w13192675>

Academic Editors: Andrzej Walega and Tamara Tokarczyk

Received: 21 July 2021

Accepted: 22 September 2021

Published: 27 September 2021

Publisher's Note: MDPI stays neutral with regard to jurisdictional claims in published maps and institutional affiliations.



Copyright: © 2021 by the authors. Licensee MDPI, Basel, Switzerland. This article is an open access article distributed under the terms and conditions of the Creative Commons Attribution (CC BY) license (<https://creativecommons.org/licenses/by/4.0/>).

1. Introduction

As an important driver of thermohaline circulation, the Nordic Sea overflow has a profound impact on environmental changes in the Arctic and even the world. In the Nordic Sea, high-density water bodies with a geopotential density (σ_θ) greater than 27.8 kg/m^3 and shallower than the Greenland-Scotland Ridge (GSR) depth can overflow. There are three overflow channels on the GSR. From west to east, they are the Denmark Strait (DS), the Iceland-Faroe Ridge (IFR), and the Faroe-Shetland Channel (FSC) (Figure 1a,b). The overflow of dense water between Greenland and Shetland consists of the Faroe Bank Channel (FBC) overflow and Wyville Thomson Ridge (WTR) overflow, and FBC is the main channel for FSC overflow. The high-density water overflowing from these channels forms the North Atlantic Deep Water (NADW), which affects the nature of the deep-water mass and the deep circulation in the North Atlantic [1–4].

Theoretical analysis and field measurement results show that the Nordic Sea overflow is hydraulically controlled. In hydraulic control theory, changes of the overflow flux through a strait depend only on the total pressure difference at the depth of the sill on both sides of the GSR [1–4]. The total pressure difference is equal to the barotropic pressure difference plus the baroclinic pressure difference, depending on the local and remote physical processes, such as convection, mixing, and circulation, which further determine the overflow flux of the Nordic Sea [4].

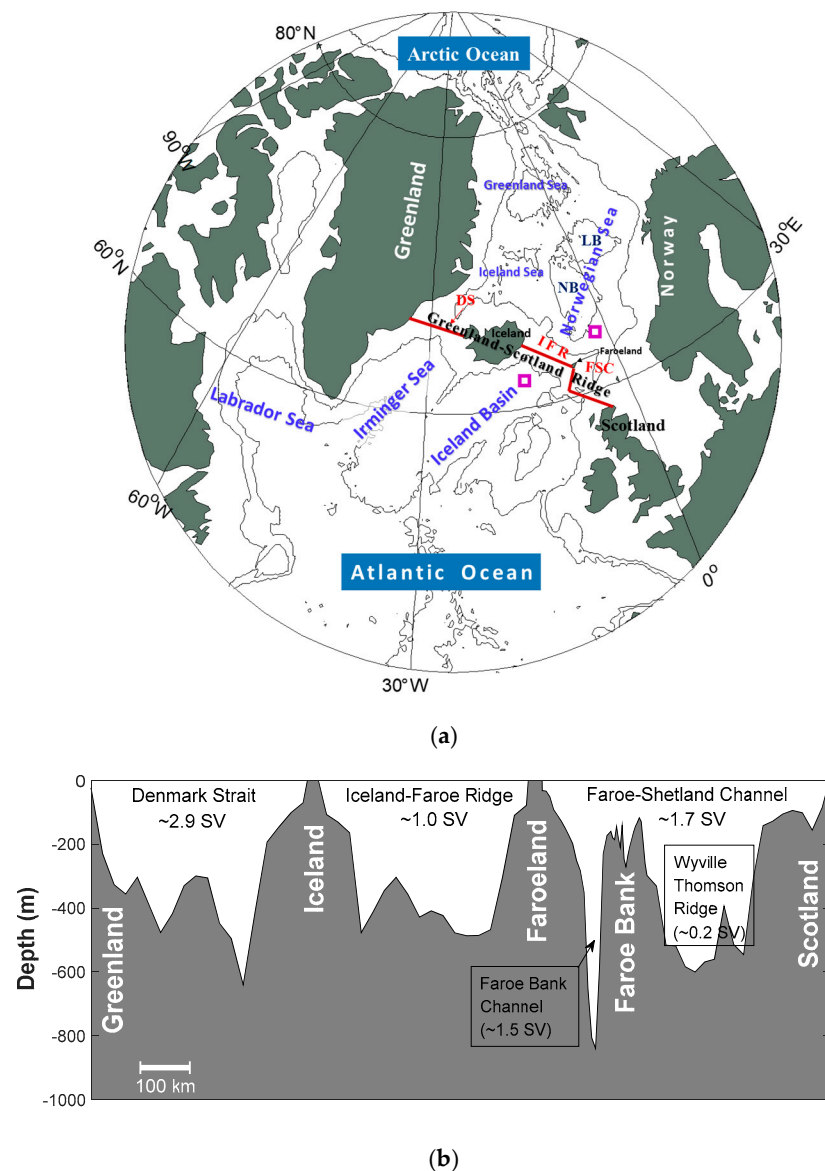


Figure 1. (a) Topographic map of the Nordic Sea and (b) bottom depth map of the GSR. Note: The Nordic Sea is composed of the Norwegian Sea, the Icelandic Sea, and the Greenland Sea. In the Norwegian Sea, LB stands for the Lofoten Basin and NB stands for the Norwegian Basin; the DS, IFR, and FSC stand for the three main overflow channels in Greenland-Scotland Ridge, namely Denmark Strait, Iceland-Farø Ridge, and Farø-Shetland Channel, respectively; the purple square represents the selected point for calculating the pressure difference between the two sides of the GSR; the red line is the selected section for the bottom depth map. Bottom depth of the oceanic part of the GSR and overflow flux are based on Hansen and Østerhus [2].

Affected by climate change, the deep convection in the Nordic Sea has been weakened significantly from the 1960s to the beginning of the 21st century; by about 2006, the depth of deep convection in Greenland was less than 1000 m [5,6]. Recent studies showed that although there is a decreasing trend in atmospheric forcing from 1993 to 2016, the depth of convection in the Greenland Sea in winter has a deepening tendency. This is due to the increase in the salinity of seawater in the upper 1500 m, which results in the weakening of stratification inside the Greenland Sea circulation [7,8]. Modern climate models have found that the overflow flux of the Nordic Sea has a good consistency with the Greenland Sea convection, showing a weakening trend [9–12]. However, this weakening is not reflected by the measured data. The field measurement found that the overflow flux of the Nordic

Sea remained strong and stable from 1995 to 2015, and there was no significant trend change [13,14].

For the phenomenon of stable overflow transport of the Nordic Sea during the last two decades, there have been studies explaining it from different aspects. Based on the model results, Olsen et al. [4] pointed out that the upper interface of the overflow water in the Nordic Sea declined from 1948 to 2005, which would cause a decrease in the pressure difference on both sides of the GSR. However, the rising sea level of the Nordic Sea offsets this effect, resulting in no trend change in the total pressure difference on both sides, making the overflow flux stable. Some other studies showed that the circulation of the Atlantic waters in the Nordic Sea has a greater impact on overflow changes, and the impact of weakened convection has been concealed [15]. Zhang and Thomas [16] believed that the Arctic Ocean, rather than the Greenland Sea, is the northern end of the mean Atlantic Meridional Overturning Circulation (AMOC). They further pointed out that the deep convection of the Labrador Sea and the Greenland Sea contribute the least to the mean AMOC, and AMOC may not be significantly weakened by the closure of the deep convections. However, some other studies still believed that the Greenland Sea is the main source area of the densest overflow water into the North Atlantic after 2005 and is the main ventilation area of the deepest layer in the North Atlantic [7,17]. Other studies suggest that the volume of the dense water above the GSR sill depth in the Nordic Seas is sufficient to supply decades of overflow transport without dense water production [1–3]. The premise in such estimations, however, is that all dense water above the sill depth is freely available for overflow transport. However, basin-scale oceanic circulation is nearly geostrophic and its streamlines are basically the same as the isobaths. The vast majority of the dense water is stored inside the closed geostrophic contours in the deep basin and thus is not freely available for overflow transport [18]. Therefore, an external force or a non-geostrophic mechanism is required to help transport the interior water mass to the boundary current. The numerical simulation results of Yang and Pratt [19] show that 80%–85% of the dense water above the GSR sill depth in the Nordic Seas is not freely available for overflow transport, and the amount of the dense water freely available to overflow accounts for only 15%–20%. Therefore, the Nordic Seas has a relatively small capacity as a dense water reservoir and thus the overflow transport is sensitive to climate changes.

In short, there is still controversy about the reasons for the stable overflow flux in the past two decades. Based on the satellite altimeter data and the reanalysis hydrological data, this paper will analyze the changes in the barotropic pressure and baroclinic pressure on both sides of the GSR and then discuss the reasons for the long-term stable flux of the Nordic Sea overflow by the hydraulic control theory.

The structure of this paper is as follows. Chapter 2 introduces the data and the method for calculating the pressure. Chapter 3 evaluates the credibility of the EN4 data to calculate the pressure by comparing the measured hydrological data and the overflow flux results. Chapter 4 mainly analyzes the spatial distribution of the change trends of the positive pressure, baroclinic pressure, and total pressure on both sides; the change characteristics of the pressure difference on both sides of the GSR; the changes in depth of the overflow water interface in the Nordic Sea; and then analyzes the reasons for stable overflow flux from 1993 to 2015. Chapter 5 mainly analyzes the correlation between the positive pressure and baroclinic pressure on both sides of the GSR and the role of the changes in the properties of the upper seawater. Chapter 6 is the conclusion.

2. Data and Methodology

2.1. Satellite Altimeter Data

The Sea Level Anomaly (SLA) data in this paper is monthly averaged data from 1993 to present of the DUACS 2014 database from the French Space Research Center (CNES), which is merged with multi-satellite altimetry data (Available online: <http://www.avisioceanobs.com/duacs/> (accessed on 5 May 2016)). The data use Mercator projection with a horizontal resolution of $1/4^\circ \times 1/4^\circ$, and are corrected by atmospheric pressure correction,

tide correction, and dry tropospheric correction. The SLA data of DUACS 2014 are based on the Mean Sea Surface (MSS) from 1993 to 2012. Since the mean sea level is the height on a fixed earth reference ellipsoid, the SLA contains sea level change signals caused by the relative crustal movement during this period, mainly as the Glacial Isostatic Adjustment (GIA). Tamisiea and Mitrovica [20] gave the distribution map of the GIA effect on the sea level change measured by the altimeter (their Figure 3b), and their results showed that the GIA has an effect of no more than 0.15 mm/yr on the sea level change trend in the Nordic Sea, so it can be ignored here. Volkov and Pujol [21] verified through field measurement that AVISO's altimeter data can be used to study sea level changes and surface currents in the Nordic Sea.

2.2. Hydrological Data

The hydrological data in this paper are the monthly averaged reanalysis data of the EN4 hydrological data set of the Met Office [22]. The data are obtained from a large amount of observational data, mainly including WOD data (World Ocean Database), GTSP data (Global Temperature and Salinity Profile Project), Argo data, and ASBO (Arctic Synoptic Basin-wide Observations) data, which have high credibility. The horizontal resolution of the data is $1^\circ \times 1^\circ$, and the coverage area is $1^\circ \text{ E}–360^\circ \text{ E}$ and $83^\circ \text{ S}–89^\circ \text{ N}$. The data has 42 vertical layers, and the thickness of the water layer ranges from 10 m in the upper layer to 300 m in the deep ocean.

Since the grid of SLA is inconsistent with the hydrological data grid, the SLA data needs to be interpolated to the same grid point as the hydrological data. The interpolation method is used to obtain the mean value of the 16 SLA grid points in each hydrological grid. If there are more than 8 missing values in a SLA data grid, the mean value at that point is also assigned as missing.

The hydrological observation data of the “Mike” station (Ocean Weather Ship Station Mike, here referred to as OWS-M station) comes from the European Ocean Observatory Network (Euro SITES, Available online: <http://www.eurosites.info/stationm.php> (accessed on 26 December 2016)). The station is located in the center of the Norwegian Sea (66° N , 02° E) and provided long-term ocean and meteorological profile data almost daily from October 1948 to November 2009.

2.3. Method for Calculating Pressure

Based on the hydrostatic assumption, the pressure at a certain depth without considering the atmospheric pressure is:

$$P = P_{\text{trop}} + P_{\text{clin}} = \rho_0 g \zeta + g \int_z^0 \rho dz \quad (1)$$

where P_{trop} represents the barotropic pressure and P_{clin} is the baroclinic pressure; $\rho_0 = 1028 \text{ kg/m}^3$ is the surface seawater density; $g = 9.8 \text{ m/s}^2$ is the gravitational acceleration; ζ is the sea level height, and here is taken as SLA; ρ is the seawater density, which is derived from the temperature and salt data of EN4; z is the calculated pressure depth, and unless otherwise specified, it is taken as 840 m, which is the maximum depth of the GSR sill. Actually, the mean sea surface level is not horizontal, and the spatial difference is huge. However, since this article focuses on the temporal change of pressure rather than the absolute value, taking ζ as the Sea Level Anomaly (SLA) will not affect the final analysis result.

3. Applicability Analysis of EN4 Data

3.1. Comparison with Observations at OWS-M Station

Analysis of the data from the OWS-M station shows that there are enough data for P_{clin} calculations every month above 1000 m depth. The monthly and annual mean results of P_{clin} calculated from the data are shown in Figure 2. Comparing the results of EN4

data with the results of EN4 data, their annual mean change curves have a high degree of overlap. The decline rate of annual mean P_{clin} at the OWS-M station during 1949–2009 was $-0.55 \pm 0.26 \times 10^2 \text{ Pa/dec}$, while the EN4 data was $-0.3 \pm 0.26 \times 10^2 \text{ Pa/dec}$, consistently showing a downward trend. Considering the annual mean P_{clin} at the OWS-M station had some missing data, the difference in the decline rate between the two data sets may have been caused by the missing data.

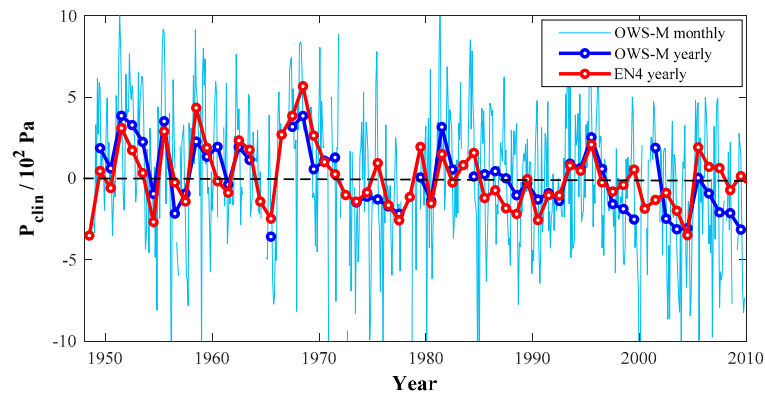


Figure 2. The P_{clin} anomaly from OWS-M data and EN4 data. Note: The OWS-M station data are the daily profile observation results. Firstly, the monthly mean temperature and salinity values at different depths are obtained by averaging, and then the monthly mean P_{clin} (at 840 m depth) is calculated from temperature and salinity; when the cumulative observation level of a month is less than 10 layers or the observation depth is less than 80 data 0 m, the month will be treated as a missing measurement. The annual mean P_{clin} of the OWS-M station is obtained from the monthly data average. A year is regarded as a missing year if there are more than 4 months in the year of missing annual mean data and is not shown.

3.2. Compared with the Observed Overflow Transport

Based on mooring ADCP and temperature and salinity observations, Hansen and Østerhus [3] found that there was no significant trend change in FBC overflow flux from 1995 to 2005, and the trend change did not exceed 0.2 Sv, which is only 10% of the mean flow. Figure 3a–c shows that the SLAs on both sides of the GSR are both increased during this period, while the P_{clin} at the depth of 840 m is decreased at the same time. The final P obtained has no remarkable trend change in the Norwegian Sea or in the Icelandic Sea. Therefore, the trend changes characteristics of the FBC overflow obtained from SLA and EN4 data are more credible.

The measured data show that the trend of DS overflow flux in the 15-year period from 1996 to 2011 is -0.4 Sv . However, the trend is below the 70% confidence level of the t -Test, so it is not significant [23]. Here the pressure at the depth of 640 m (approximately the depth of DS) on the north and south sides of the DS increases by the same magnitude, and the pressure difference between the two sides is basically unchanged. The spatial distributions of P_{clin} and P at the depth of 640 m are basically the same as in Figure 2a–c, which is not shown separately here. Thus, the calculation results here are consistent with the observation.

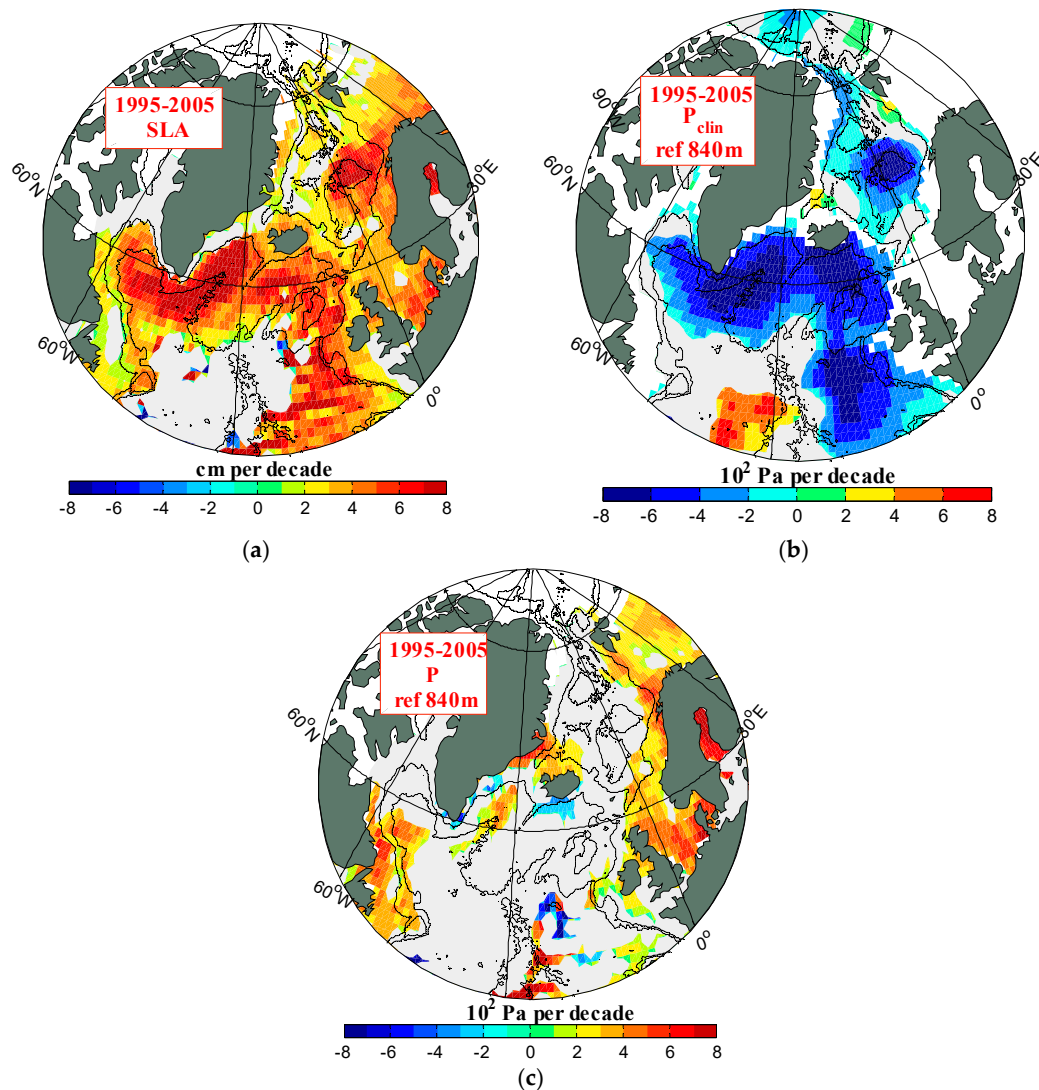


Figure 3. The change trend of SLA (a), P_{clin} (b), and P (c) from 1995 to 2005. The gray area represents the sea area that has not passed the 95% significance test; the white area represents the sea area where the period of missing data is longer than 7 years; the black lines are the 1000 and 3000 m isobaths. The pressure is calculated based on a reference depth of 840 m.

4. Change from 1993 to 2015

In the published literatures, the observation of GSR overflow flux is available until 2015 [14]. Since the Nordic Sea overflow is hydraulically controlled, the pressure difference on both sides of the GSR can be used to analyze the long-term changes of the overflow flux. The depth of the deepest GSR sill is about 840 m on the FBC, which can be used to calculate the pressure difference [4]. As shown in Figure 4, from 1993 to 2015 the SLAs of the Nordic Sea and the North Atlantic subpolar region near the GSR basically increased at the same rate; P_{clin} mostly declined in the south of GSR, increased near DS in the north of GSR, and had no significant change in the south of Norwegian Basin. The pressure difference in the west of Iceland had a clear upward trend; the pressure difference to the east of Iceland was basically unchanged. This means that DS overflow increased, while FBC overflow and IFR overflow did not change much. Therefore, the total overflow in the Nordic Sea slightly increased.

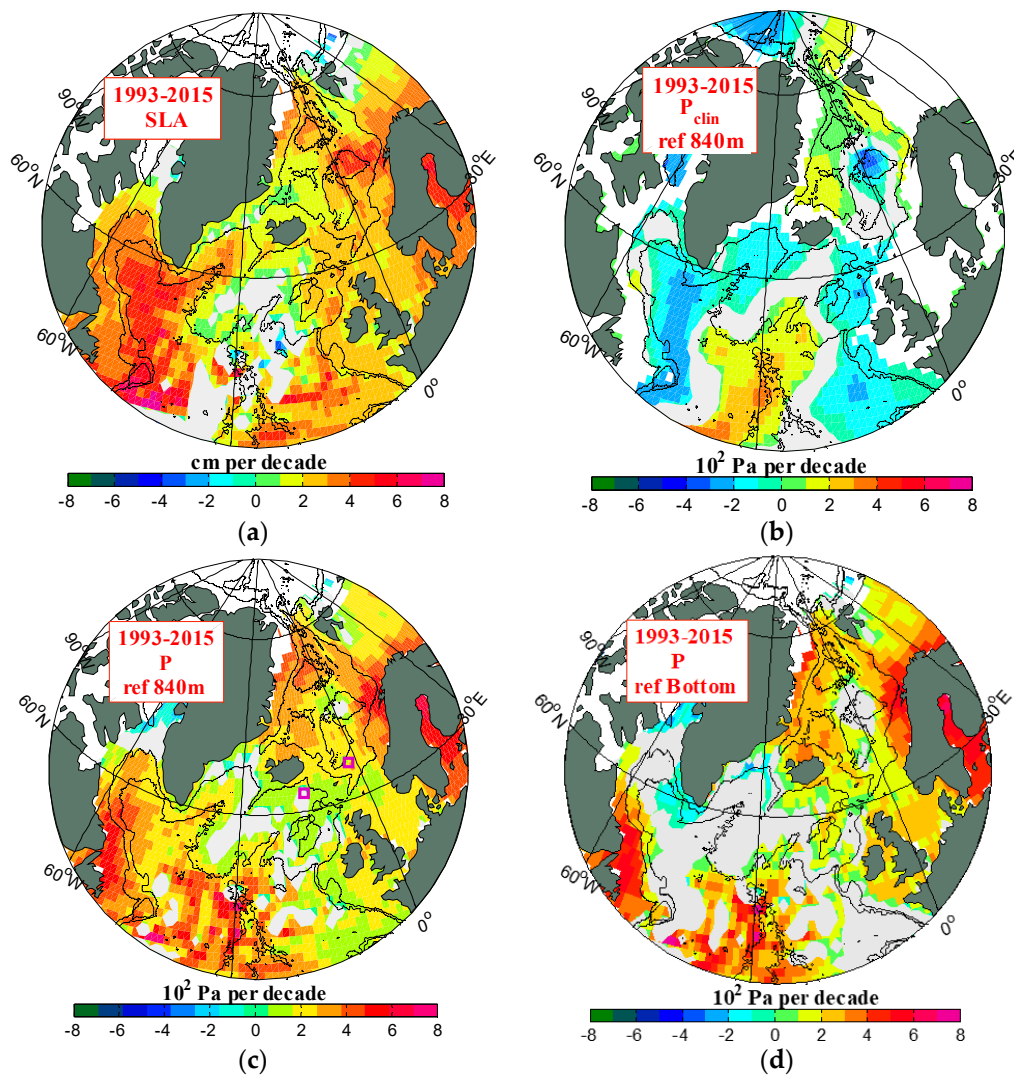


Figure 4. SLA (a), P_{clin_840} (b), P_{840} (c), P_{bottom} (d) changes trends from 1993 to 2015. The gray area represents the sea area that has not passed the 95% significance test; the white area represents the sea area where the period of missing data is longer than 7 years. The black lines are the 1000 and 3000 m isobaths; the purple square represents the selected point for calculating the pressure difference between the two sides of the GSR in panel (c).

In the Nordic Sea, the depth of $\sigma_\theta = 27.8 \text{ kg/m}^3$ ($D_{27.8}$) (Figure 5a,b, the upper interface of the overflow water) is more consistent with the spatial distribution of the change rate of P_{clin} , indicating that changes in the properties of the upper seawater necessarily indicate the adjustments of the upper interface of the overflow water. Especially in the Nordic Sea, the sinking of $D_{27.8}$ in the Lofoten Basin is about 100 m/dec, which may be directly caused by the reduction of deep convection in the Greenland Sea [5,6] or the weakening of other dense water production. When the total overflow transport flux remains unchanged, the amount of overflow water flowing out of the Lofoten Basin almost remains unchanged. Therefore, the reduction of dense water supply leads to the rapid sinking of the overflow water interface in the Lofoten Basin. There, the rapid decline of P_{clin} and the rapid rise of P_{trop} occur at the same time, while P is basically unchanged, indicating that the above changes are probably caused by the change of physical property of the upper water.

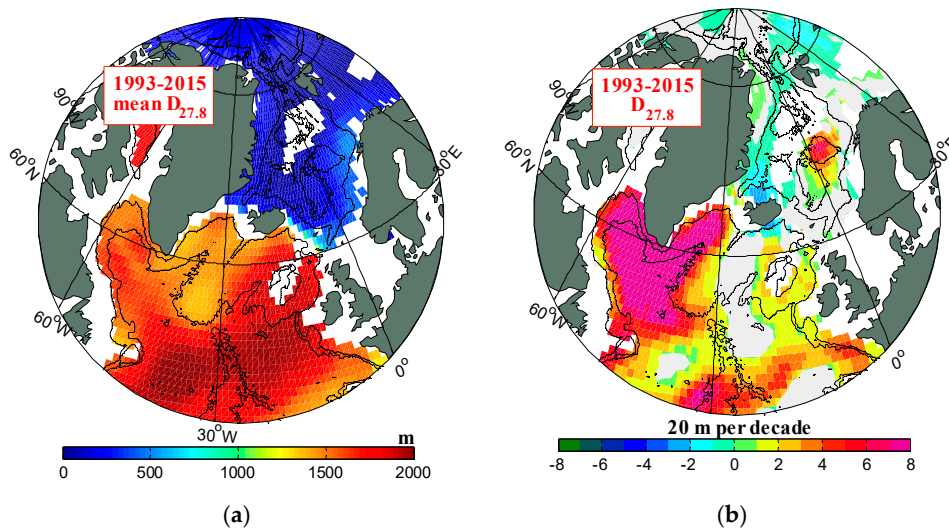


Figure 5. The spatial distribution of the mean value (a) and change rate (b) of $D_{27.8}$ from 1993 to 2015. The $D_{27.8}$ is the depth of $\sigma_{\theta}=27.8 \text{ kg/m}^3$.

The Labrador Sea is a fast-sinking area of $D_{27.8}$, with a sinking rate up to 160 m/dec or more, which is consistent with the reported weakening of convection there [24,25]. In the modern climate, the Nordic Sea overflow, entrainment process, and Labrador Sea convection provides about 1/3 of the deep branch of the radial overturning circulation in the Atlantic Ocean [4,26]. Under the condition that the overflow of the Nordic Sea is relatively stable, the convection in the Labrador Sea is significantly weakened, which may be the main reason for the significant weakening of the AMOC near 25° N [24,27]. However, some relatively new observational evidence has indicated that the deep convection of the Labrador Sea has the smallest total contribution to the subpolar overturning circulation [28,29].

The convection of the Labrador Sea is significantly weakened, which causes the upper interface of the dense water to sink quickly. Since the upper interface of the overflow water in the Labrador Sea is deeper than 1500 m, its impact on the P_{clin} at 840 m is small, and the decrease rate of P_{clin} at 840 m depth is only $-2 \times 10^2 \text{ Pa/dec}$. The deepening of the overflow water in the Labrador Sea means that warming and freshening of the entire water column causes a large increase in SLA, which is consistent with the calculated results. The greater the bottom depth is, the greater the increase of SLA is. However, there is no significant trend change in the mass of the entire water column from surface to the bottom (Figure 4d).

Although the changes in properties of seawater can ensure the mass conservation of the whole water column, the compression or expansion of the water column caused by the change of properties of seawater will lead to the change of the mass ratio of the upper and lower water column at a certain depth. Therefore, in hydrostatic balance, the pressure change of seawater at a certain depth may be caused by the change of properties of seawater below this depth, and the change of properties of seawater above this depth has no effect on it. The different changing trends of the pressure at 840 m depth and the seabed depth in the Labrador Sea and the Irminger Sea in the south of Greenland (Figure 4b,d) show this effect.

Two points have been selected at the upstream and downstream ends of the FBC to construct the temporal variations of pressure difference. Based on the overflow water sources in different overflow channels and combining the location given by Olsen et al. [4], we selected ($64^{\circ} \text{ N}, 2^{\circ} \text{ W}$) and ($62^{\circ} \text{ N}, 15^{\circ} \text{ W}$) to estimate the FBC overflow flux (the location is shown in Figure 1). It can be seen from Figure 6 that the inter-annual variation characteristics of ΔP_{trop} and ΔP_{clin} obtained in this paper are very consistent with Figure 2 of Olsen et al. [4]. Both results showed the minimum values of ΔP_{clin} and ΔP in 1995, and

the relative maximum values of ΔP_{trop} and ΔP in 2003; from 1993 to 2005, ΔP_{clin} and ΔP were rapidly rising and ΔP_{trop} had no significant change trend. At the same time, the inter-annual variation of ΔP calculated here is about 2×10^2 Pa and about 10% of the mean ΔP , which is basically consistent with the observed inter-annual variation of FBC overflow [3]. In short, the pressure difference between the two points selected in this paper can be used to estimate the FBC overflow flux change. From the spatial distribution map of the SLA trend rate (Figure 4), it can be seen that the trend rate of SLA has a good spatial continuity in the sea areas near both sides of the GSR, and the results would not be significantly changed due to slight difference in the selection of the grid location.

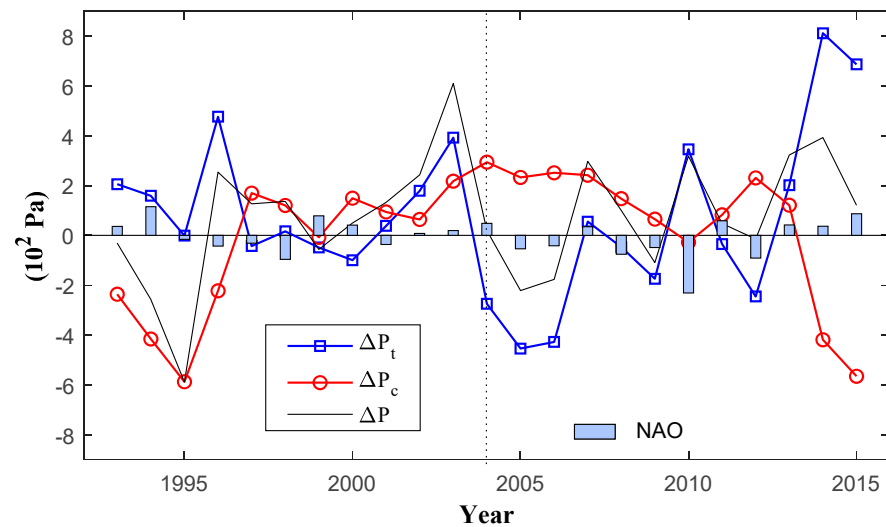


Figure 6. The variations of annual mean of ΔP_{trop} , ΔP_{clin} , and ΔP . The positions of the selected grid points to calculate pressure difference on both sides of the GSR are shown in Figure 1.

Specifically, ΔP_{trop} experienced a slow decline with fluctuation from 1993 to 2005 and reached the minimum value in the past 23 years before 2005. ΔP_{trop} increased with fluctuation from 2005 to 2013 and rose rapidly from 2013 to 2014; after that, it fell back. The year 2014 had the maximum value of ΔP_{trop} in the past 23 years (Figure 6). ΔP_{clin} first decreased slightly in the period of 1993–1997, then increased before 2004, and reached the maximum value in the past 23 years before 2004; then it decreased slowly in the period of 2004–2013, and decreased rapidly in the last two years. ΔP_{clin} in 2015 reached the minimum value in the past 23 years. ΔP was basically at an average level in 1993, followed by a relatively large fluctuation. After experiencing the minimum value in 1995 and the maximum value in 2003, it basically returned to the mean level in 2015. The linear regression of the annual mean ΔP results in a change rate of 1.6×10^2 Pa/dec. Olsen et al. [4] gave a linear coefficient of FBC overflow flux change (Δq) and ΔP of $k = 10^{-3}$ Sv/Pa. Using this linear coefficient, we obtain the FBC overflow enhancement rate of about 0.16 Sv/dec, which is quite small relative to the mean FBC overflow flux (2.9 Sv). At the same time, the linearly increasing trend of ΔP failed the 95% confidence test but passed the 90% confidence test. In fact, ΔP in 2015 was only about 1×10^2 Pa larger than in 1993, which is quite small.

The changes in these three parameters have no significant correspondence with NAO, and most of the wind stress curl changes in the Nordic Sea are related to NAO [30]. This indicates that the interannual sea level changes are not mainly driven by wind stress, but more likely are the result of changes in the properties of the upper seawater.

5. Relationship between Barotropic Pressure and Baroclinic Pressure

Olsen et al. [4] concluded that ΔP_{trop} and ΔP_{clin} on both sides of the FBC have a correlation lag of about three years, and analyzed the mechanism of the correlation as follows: due to wind stress, the sea level difference on both sides of the FBC increases

(decreases) and the ΔP on both sides increases (decreases) through the barotropic pressure effect. Then, the overflow transport is enhanced (weakened), causing the iso-density interface in the Norwegian Basin to sink (rise) and the ΔP_{clin} gradually decreases (increases); and then ΔP gradually decreases (increases) until recovers to normal level. This feedback mechanism could help ΔP remain stable, which means the overflow transport is stable. They use a simplified two-layer model to express the mechanism as:

$$P_{\text{trop}} = \rho_0 g \Delta h \quad (2)$$

$$\Delta P_{\text{clin}} = -g \Delta \rho \Delta D \quad (3)$$

$$\Delta P_{\text{clin}} = -g \Delta \rho \Delta D = \frac{-g \Delta \rho k T}{A} \Delta P_{\text{trop}} \quad (4)$$

where $\rho_0 = 1.025 \times 10^3 \text{ kg/m}^3$ is the surface seawater density, $g = 9.8 \text{ kg/m}^3$ is the gravitational acceleration, and $\Delta \rho = 0.5 \text{ kg/m}^3$ is the density difference between overflow water and upper water body. Linear regression coefficient of overflow flux change (Δq) and pressure difference (ΔP) is $k = 10^{-3} \text{ Sv/Pa}$. A is the contact area between the overflow layer and the upper layer in the Nordic Sea, or rather the area of the Norwegian Sea deeper than 500 m, which is equal to $5.8 \times 10^{11} \text{ m}^2$ [4]. T is the time for the high-density water interface to sink ΔD after the barotropic pressure disturbance, which is also the time for ΔP to restore to the initial state. The calculated T is approximately equal to three years.

The monthly mean variation of ΔP_{trop} , ΔP_{clin} , and ΔP was constructed based on EN4 and SLA data, and the correlation between ΔP_{trop} and ΔP_{clin} lagging or leading in different months was analyzed (Figure 7). When ΔP_{trop} is about three months ahead of ΔP_{clin} , the negative correlation between them is the largest (-0.59). Olsen et al. [4] defined the horizontal spatial area occupied by overflow water as the seabed deeper than 500 m. However, the dense water in the Norwegian Sea is not freely available for overflow transport, and the dense water in the center of the basin, which occupies most of the area, is circulated by the boundary oceanic circulation. Therefore, the size of the effective overflow area is much smaller than that of the ocean basin. Based on the feedback mechanism of Olsen et al. [4] and the lag time obtained in this article, the horizontal spatial range of available overflow water upstream of the FBC can be estimated to be $0.5 \times 10^{11} \text{ m}^2$, which is about 1/12 of the value given by Olsen et al. [4]. This ratio is close to the percentage of available overflow water in the total overflow water in the Nordic Sea (80%~85%) obtained by other studies [19].

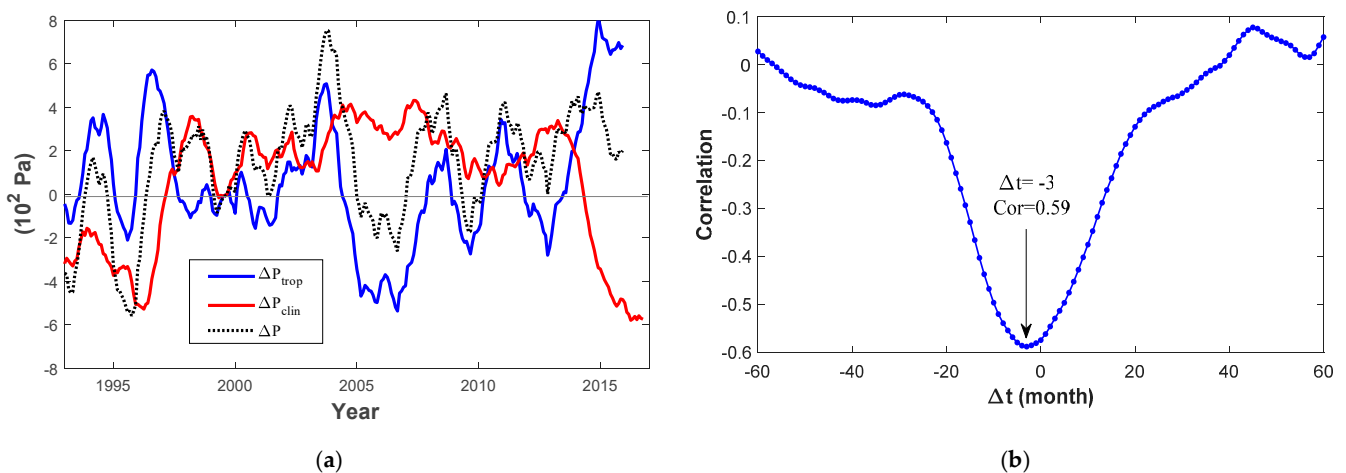


Figure 7. The variation (a) and the correlation for different lag time lengths (b) of ΔP_{trop} and ΔP_{clin} .

The high P_{clin} correlation with the station in the southern part of the Norwegian Sea (64 N, 2 W) is limited to a small area in the southern part of the Norwegian Sea (the area

with a correlation greater than 0.8 in Figure 8). The P_{clin} in this area has a good consistency of change, which can be considered as the available overflow area upstream of the FBC overflow. The area with a correlation greater than 0.8 is about $1.8 \times 10^{11} \text{ m}^2$, and the area with a correlation greater than 0.9 is $0.9 \times 10^{11} \text{ m}^2$. It is more likely that the changes of ΔP_{trop} and ΔP_{clin} are both dominated by changes in seawater properties, so the largest negative correlation between them basically has no lead or lag (Figure 9).

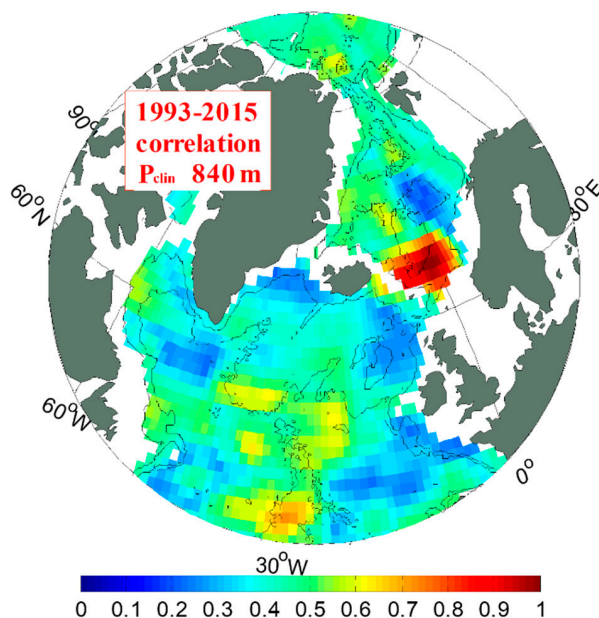


Figure 8. The correlation between P_{clin} and P_{clin} at selected stations in the Norwegian Sea. The time series of the correlation analysis has undergone a 12-month moving average processing. The correlation here is the maximum correlation within 5 years of lead or lag time. The selected stations in the Norwegian Sea are shown in Figure 1 as a purple square. The time series of ΔP_{trop} , ΔP_{clin} , and ΔP are all carried on a 12-month moving mean to remove seasonal fluctuations in this figure. For the sake of comparison, ΔP_{clin} and ΔP are shown as anomalies.

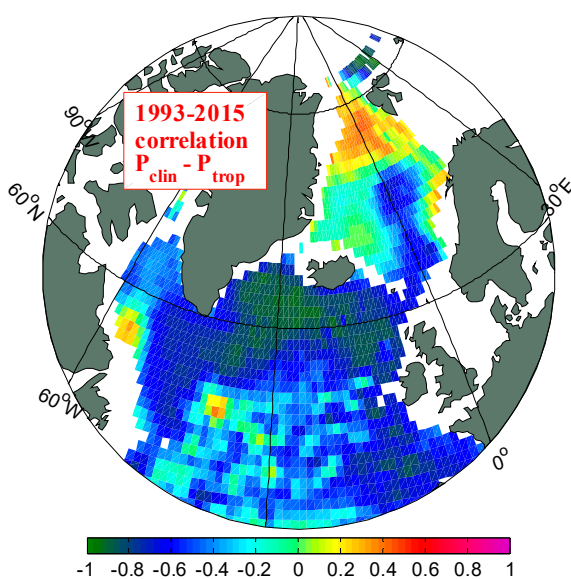


Figure 9. The correlation between P_{clin} and P_{trop} .

Changes in the properties of the upper seawater will cause the reverse change of P_{clin} and P_{trop} , while the total pressure will not change due to the unchanged seawater

quality. Therefore, the sea area with a stronger negative correlation between P_{clin} and P_{trop} indicates that changes in the properties of the upper seawater play a greater role in the changes of both there. It can be seen from Figure 9 that there is a strong negative correlation between P_{clin} and P_{trop} in the southern sea area of GSR, the correlation coefficient is close to -1.0 , while the total pressure at this place has no trend change characteristics (Figure 4), which shows that the changes of P_{clin} and P_{trop} are mainly caused by the changes in the properties of the upper seawater. In the Nordic Sea north of GSR, this negative correlation is not so strong. Among them, in the Norwegian Sea, P_{clin} and P_{trop} have a certain negative correlation, indicating that the change in the properties of the upper seawater is one of the important factors which cause the changes in the two. There are other processes that lead to the increase in the quality of the upper seawater, which causes a slight increase trend in the total pressure (Figure 4). The negative correlation between P_{clin} and P_{trop} is no longer significant in other areas of the Nordic Sea except the Norwegian Sea. In the Icelandic Sea, the correlation between P_{clin} and P_{trop} is poor and the SLA increases significantly, which leads to a significant increase in the total pressure (Figure 4). There is a weak positive correlation between the two in the Greenland Sea, indicating that the changes of P_{clin} and P_{trop} in this area are mainly affected by other processes.

Under hydrostatic assumption, changes in the density of seawater above 840 m depth will not change the hydrostatic pressure at this depth. To change the pressure at this depth, it needs to change the mass of the water column at this depth. There are two ways. One is to change the absolute mass of the water column, or to change the sea level through wind stress curl, runoff input, sea-air material flux, and other factors. The other is to change the relative mass of the water column by changing the density of the deep layer, causing the column to expand or contract. The mass percentage of the water column above the 840 m depth can change the entire water column.

At present, most ocean numerical models are based on Boussinesq approximation, which cannot reflect sea level changes caused by changes in seawater properties. When the density of the sea layer in Northern Europe decreases, the pressure obtained by simulation decreases, which in turn leads to the weakening of simulated overflow [31]. It can be seen from the results of this paper that the steric effect contributes to most of the sea level trend changes in the sea area surrounding the GSR and has a significant impact on the long-term changes in overflow transport. Therefore, the simulation and prediction of long-term changes in overflow requires the use of non-Boussinesq ocean models, considering the impact of changes in seawater properties on SLA.

6. Conclusions

The Nordic Sea overflow is hydraulically controlled; the changes of the overflow flux depend only on the pressure difference at the depth of the overflow outlet on both sides of the GSR. Based on the satellite altimeter data and the reanalysis hydrological data, we obtained a slight increase in the pressure difference between the two sides of the GSR from 1995 to 2015. However, this trend is not significant and is more consistent with the observed stable overflow flux. Among them, the barotropic pressure and baroclinic pressure in the southern sea area of the GSR have a very good negative correlation (correlation coefficient is close to -1.0). The changes in both are basically caused by the changes in the properties of the upper seawater, and the total pressure there is only a slight increasing trend. The barotropic pressure and baroclinic pressure of the Norwegian Sea in the northern part of the GSR have a certain negative correlation (correlation coefficient is about -0.6), indicating that changes in the properties of the upper seawater are important factors that cause changes in the barotropic and baroclinic pressures in the sea area, and other processes can also lead to a slight increase in the barotropic pressure there. While the correlation between the barotropic pressure and the baroclinic pressure in the Icelandic Sea is poor, the barotropic pressure increases significantly which leads to a significant increase in the total pressure there.

By selecting two representative points, the barotropic pressure difference and baroclinic pressure difference on both sides of the FBC are constructed. The changes in the barotropic pressure and baroclinic pressure on both sides of the FBC are more likely caused by the changes in the properties of the local upper seawater. The total pressure difference caused no significant trend changes characteristics between 1993–2015, which is consistent with the observation of stable overflow flux.

In the Nordic Sea, the area with the fastest sinking of the overflow water upper interface is the Lofton Basin, with a sinking speed of more than 100 m/dec, indicating that the storage of overflow water there is rapidly decreasing. The physical processes that produce dense water, such as deep convection in the Greenland Sea, are weakening, and the source of overflow provided is reducing, leading to warming and lightening of the upper layer of the Norwegian Sea and sinking of the upper interface of the overflow water. However, the changes in the properties of the upper seawater in the Norwegian Sea cannot reduce upstream pressure in the depth of the sill to weaken overflow transport. Therefore, it will cause the upper interface of upstream overflow water to further decrease. In the future, when the depth of the overflow water upper interface in the Nordic Sea is less than the depth of the sill on the GSR, the overflow may greatly slow down or even experience a hiatus. This is worthy of close attention and further study.

Author Contributions: Conceptualization, W.S.; methodology, W.S. and N.L.; software, W.S. and X.L.; formal analysis, W.S.; writing—original draft preparation, W.S.; writing—review and editing, N.L.; supervision, X.L.; Funding acquisition, W.S. and X.L. All authors have read and agreed to the published version of the manuscript.

Funding: This research was funded by the National Natural Science Foundation of China, grant number 41806219 and 41806002, the National key research and development program, grant number 2018YFC1407602 and 2019YFC1408405, and the Youth Science and Technology Star Project of Dalian (2020RQ020).

Institutional Review Board Statement: The study did not involve humans or animals.

Informed Consent Statement: We choose to exclude this statement as the study did not involve humans.

Data Availability Statement: The sea level anomaly (SLA) data in this paper are monthly averaged data from 1993 to present of the DUACS 2014 database from the French Space Research Center (CNES), which is merged with multi-satellite altimetry data (<http://www.avisioceanobs.com/duacs/> accessed on 24 September 2021). The monthly mean reanalysis data of the EN4 hydrological data set are from Met Office Hadley Centre observations data sets (<https://www.metoffice.gov.uk/hadobs/en4/> accessed on 24 September 2021).

Conflicts of Interest: The authors declare no conflict of interest.

References

1. Käse, R.H. A Riccati model for Denmark Strait overflow variability. *Geophys. Res. Lett.* **2006**, *33*, 21. [[CrossRef](#)]
2. Hansen, B.; Østerhus, S. North Atlantic–nordic seas exchanges. *Prog. Oceanogr.* **2000**, *45*, 109–208. [[CrossRef](#)]
3. Hansen, B.; Østerhus, S. Faroe bank channel overflow 1995–2005. *Prog. Oceanogr.* **2007**, *75*, 817–856. [[CrossRef](#)]
4. Olsen, S.M.; Hansen, B.; Quadfasel, D.; Østerhus, S. Observed and modelled stability of overflow across the Greenland–Scotland ridge. *Nature* **2008**, *455*, 519–522. [[CrossRef](#)]
5. Latarius, K.; Quadfasel, D. Seasonal to inter-annual variability of temperature and salinity in the Greenland Sea Gyre: Heat and freshwater budgets. *Tellus A Dyn. Meteorol. Oceanogr.* **2010**, *62*, 497–515. [[CrossRef](#)]
6. Tverberg, V.; Pavlov, V.; Hansen, E.; O'Dwyer, J. Decadal trends in exchange of heat, salt and deep water between the Arctic Ocean and the Nordic Seas. In Proceedings of the ICES Annual Science Conference, 2001, Oslo, Norway, 26–29 September 2001.
7. Brakstad, A.; Våge, K.; Håvik, L.; Moore, G.W.K. Water mass transformation in the Greenland Sea during the period 1986–2016. *J. Phys. Oceanogr.* **2019**, *49*, 121–140. [[CrossRef](#)]
8. Lauvset, S.K.; Brakstad, A.; Våge, K.; Olsen, A.; Jeansson, E.; Mork, K.A. Continued warming, salinification and ox-ygenation of the Greenland Sea gyre. *Tellus Dyn. Meteorol. Oceanogr.* **2018**, *70*, 1–9. [[CrossRef](#)]
9. Solomon, S. The physical science basis: Contribution of Working Group I to the fourth assessment report of the Intergovernmental Panel on Climate Change. Intergovernmental Panel on Climate Change (IPCC). *Clim. Chang.* **2007**, *2007*, 996.

10. Guemas, V.; Salas-Méla, D. Simulation of the Atlantic meridional overturning circulation in an atmosphere-ocean global coupled model. Part II: Weakening in a climate change experiment: A feedback mechanism. *Clim. Dyn.* **2008**, *30*, 831–844. [[CrossRef](#)]
11. Brodeau, L.; Koenigk, T. Extinction of the northern oceanic deep convection in an ensemble of climate model simulations of the 20th and 21st centuries. *Clim. Dyn.* **2016**, *46*, 2863–2882. [[CrossRef](#)]
12. Heuzé, C. North Atlantic deep water formation and AMOC in CMIP5 models. *Ocean Sci.* **2017**, *13*, 609–622. [[CrossRef](#)]
13. Chafik, L.; Rossby, T. Volume, heat, and freshwater divergences in the subpolar North Atlantic suggest the Nordic seas as key to the state of the meridional overturning circulation. *Geophys. Res. Lett.* **2019**, *46*, 4799–4808. [[CrossRef](#)]
14. Østerhus, S.; Woodgate, R.; Valdimarsson, H. Arctic Mediterranean exchanges: A consistent volume budget and trends in transports from two decades of observations. *Ocean Sci.* **2019**, *15*, 379–399. [[CrossRef](#)]
15. Eldevik, T.; Nilsen, J.E.Ø.; Iovino, D.; Olsson, K.A.; Sandø, A.B.; Drange, H. Observed sources and variability of Nordic seas overflow. *Nat. Geosci.* **2009**, *2*, 406–410. [[CrossRef](#)]
16. Zhang, R.; Thomas, M. Horizontal circulation across density surfaces contributes substantially to the long-term mean northern Atlantic Meridional Overturning Circulation. *Nat. Commun.* **2021**, *2*, 1–12.
17. Huang, J.; Pickart, R.S.; Huang, R.X.; Lin, P.; Brakstad, A.; Xu, F. Sources and upstream pathways of the densest overflow water in the Nordic Seas. *Nat. Commun.* **2020**, *11*, 1–9. [[CrossRef](#)]
18. Nøst, O.A.; Isachsen, P.E. The large-scale time-mean ocean circulation in the Nordic Seas and Arctic Ocean estimated from simple dynamics. *J. Mar. Res.* **2003**, *61*, 175–210. [[CrossRef](#)]
19. Yang, J.; Pratt, L.J. On the effective capacity of the dense-water reservoir for the Nordic seas overflow: Some effects of topography and wind stress. *J. Phys. Oceanogr.* **2013**, *43*, 418–431. [[CrossRef](#)]
20. Tamisiea, M.E.; Mitrovica, J.X. The moving boundaries of sea level change: Understanding the origins of geographic variability. *Oceanography* **2011**, *24*, 24–39. [[CrossRef](#)]
21. Volkov, D.L.; Pujol, M.I. Quality assessment of a satellite altimetry data product in the Nordic, Barents, and Kara sea. *J. Geophys. Res. Oceans* **2012**, *117*, C3. [[CrossRef](#)]
22. Good, S.A.; Martin, M.J.; Rayner, N.A. EN4: Quality controlled ocean temperature and salinity profiles and monthly objective analyses with uncertainty estimates. *J. Geophys. Res. Oceans*. **2013**, *118*, 6704–6716. [[CrossRef](#)]
23. Jónsson, S.; Valdimarsson, H. Water mass transport variability to the North Icelandic shelf, 1994–2010. *ICES J. Mar. Sci.* **2012**, *69*, 809–815. [[CrossRef](#)]
24. Robson, J.; Hodson, D.; Hawkins, E.D.; Sutton, R. Atlantic overturning in decline? *Nat. Geosci.* **2014**, *7*, 2–3. [[CrossRef](#)]
25. Yang, Q.; Dixon, T.H.; Myers, P.G.; Bonin, J.; Chambers, D.; Van Den Broeke, M.R.; Mortensen, J. Recent increases in Arctic freshwater flux affects Labrador Sea convection and Atlantic overturning circulation. *Nat. Commun.* **2016**, *7*, 1–8. [[CrossRef](#)]
26. Bailey, D.A.; Rhines, P.B.; Häkkinen, S. Formation and pathways of North Atlantic Deep Water in a coupled ice-ocean model of the Arctic-North Atlantic Oceans. *Clim. Dyn.* **2005**, *25*, 497–516. [[CrossRef](#)]
27. Srokosz, M.A.; Bryden, H.L. Observing the Atlantic Meridional Overturning Circulation yields a decade of inevitable surprises. *Science* **2015**, *348*, 6241. [[CrossRef](#)]
28. Lozier, M.S.; Li, F.; Bacon, S.; Bahr, F.; Bower, A.S.; Cunningham, S.A.; de Jong, M.F.; de Steur, L.; de Young, B.; Fischer, J.; et al. A sea change in our view of overturning in the subpolar North Atlantic. *Science* **2019**, *363*, 516–521. [[CrossRef](#)]
29. Petit, T.; Lozier, M.S.; Josey, S.A.; Cunningham, S. Atlantic deep water formation occurs primarily in the iceland basin and irmingier sea by local buoyancy forcing. *Geophys. Res. Lett.* **2020**, *47*, e2020GL091028. [[CrossRef](#)]
30. Serra, N.; Kaese, R.H.; Kähl, A.; Stammer, D.; Quadfasel, D. On the low-frequency phase relation between the Denmark Strait and the Faroe-Bank Channel overflows. *Tellus Dyn. Meteorol. Oceanogr.* **2010**, *62*, 530–550. [[CrossRef](#)]
31. Chen, X.Y.; Qiao, F.L.; Wang, X.H.; Zhao, W.; Yuan, Y.L. On the study on boussinesq approximation and hydrostatic approximation in ocean circulation. *Adv. Mar. Sci.* **2004**, *22*, 91–96.